Computer Methods in Biomechanics and Biomedical Engineering, 2013
http://dx.doi.org/10.1080/10255842.2012.746676

Taylor & Francis
Taylor & Francis Group

Simulation of transcatheter aortic valve implantation: a patient-specific finite element approach

F. Auricchio[a,b,c], M. Conti[a], S. Morganti[a]* and A. Reali[a,b]

[a]*Dipartimento di Ingegneria Civile e Architettura (DICAr), Università degli Studi di Pavia, Via Ferrata 1, 27100, Pavia, Italy;* [b]*Istituto di Matematica Applicata e Tecnologie Informatiche (IMATI-CNR), Pavia, Italy;* [c]*Centro di Simulazione Numerica Avanzata (CESNA-IUSS), Pavia, Italy*

(*Received 22 June 2012; final version received 1 November 2012*)

Until recently, heart valve failure has been treated adopting open-heart surgical techniques and cardiopulmonary bypass. However, over the last decade, minimally invasive procedures have been developed to avoid high risks associated with conventional open-chest valve replacement techniques. Such a recent and innovative procedure represents an optimal field for conducting investigations through virtual computer-based simulations: in fact, nowadays, computational engineering is widely used to unravel many problems in the biomedical field of cardiovascular mechanics and specifically, minimally invasive procedures. In this study, we investigate a balloon-expandable valve and we propose a novel simulation strategy to reproduce its implantation using computational tools. Focusing on the Edwards SAPIEN valve in particular, we simulate both stent crimping and deployment through balloon inflation. The developed procedure enabled us to obtain the entire prosthetic device virtually implanted in a patient-specific aortic root created by processing medical images; hence, it allows evaluation of postoperative prosthesis performance depending on different factors (e.g. device size and prosthesis placement site). Notably, prosthesis positioning in two different cases (distal and proximal) has been examined in terms of coaptation area, average stress on valve leaflets as well as impact on the aortic root wall. The coaptation area is significantly affected by the positioning strategy (−24%, moving from the proximal to distal) as well as the stress distribution on both the leaflets (+13.5%, from proximal to distal) and the aortic wall (−22%, from proximal to distal). No remarkable variations of the stress state on the stent struts have been obtained in the two investigated cases.

Keywords: transcatheter aortic valve; finite element analysis; patient-specific modelling

1. Introduction

Increase of life expectancy and population average age has favoured the genesis and progression of degenerative cardiovascular disease; in particular, aortic valve stenosis due to calcification is the most frequent aortic valve disorder (AHA committee 2010). In this case, surgical aortic valve replacement is the most common remedy (David et al. 1988; Peterseim et al. 1999); however, open-heart surgery with cardiopulmonary bypass is not always recommended in critically ill patients (Iung et al. 2003).

In this scenario, the development of dedicated minimally invasive techniques aimed at reducing the intra- and post-operative patient trauma and the overall recovery time and cost is certainly important (Fann et al. 2008). In particular, the introduction of catheter-based techniques to replace the aortic valve via the endoluminal path can be referred from Cribier et al. (1986), who carried out the first percutaneous transluminal valvuloplasty. Unfortunately, such a treatment provided very poor mid- and long-term outcome (Lieberman et al. 1995), and the associated risks and follow-up events have been a matter of concern (Holmes et al. 1991). However, new developments in cardiothoracic surgery have provided a significant input for such a challenging task. In fact, in 2002, Cribier carried out the first clinical implant of a percutaneous balloon-expandable aortic valve at the level of the native valve (Cribier et al. 2002), whereas in 2004, Grube implanted, for the first time, a self-expandable transcatheter valve (Grube et al. 2006). Although several devices for transcatheter aortic valve implant (TAVI) have been proposed over the last decade, two devices are now in clinical use for a few years: the Medtronic Core valve and the Edwards Lifescience SAPIEN valve. Although the Core valve is self-expandable, the Edwards Lifescience SAPIEN valve is basically composed of three flexible biological leaflets sutured on a stainless steel balloon-expandable stent. SAPIEN placement can be achieved via either a transfemoral or transapical access. In the first case, the prosthetic device is inserted through the femoral artery and passes retrogradely through the aorta until the aortic root is reached (Webb et al. 2006), whereas in the second case, it is placed directly via the apex of the heart (Lichtenstein et al. 2006). Once the device has been positioned, balloon inflation leads to valved stent expansion, which excludes and compresses the native diseased leaflets. Positioning is crucial because it affects post-operative performance: on one hand, the implanted

*Corresponding author. Email: simone.morganti@unipv.it

valve must guarantee regular flow through the coronaries, whereas on the other hand, the prosthesis should not overlap and crush the left bundle branch (Piazza et al. 2008).

Despite these new promising results and the constant technological innovation in this field, some concerns related to the limited amount of follow-up data, durability and re-intervention risks are still present. Consequently, safety, reliability and efficacy are the key issues to address for further promoting TAVI with respect to the standard surgical approach; certainly, its procedural risks differ from those related to surgical valve replacement as highlighted by Masson et al. (2009), calling for improvements in the design of devices and implantation techniques.

In this context, finite element analysis (FEA) can not only be an integral part of the design process, but also a predictive tool to clinicians during the decision-making process (Fann et al. 2008). Specifically, FEA has been used to develop new concepts for different percutaneous aortic leaflet geometries (Smuts et al. 2011) or to better understand the mechanics and haemodynamics of TAVI devices (Sun et al. 2010; Wang et al. 2012). Similarly, Schievano et al. (2010) and Capelli et al. (2010) proposed an FEA-based methodology to provide information and help clinicians during percutaneous pulmonary valve implantation planning, whereas a more recent study deals with the deployment of SAPIEN within several patient-specific aortic root models (Capelli et al. 2012).

Although these works already represent a significant step forward towards the realistic simulation of TAVI using SAPIEN-like devices, the presence of the biological valve prosthesis mounted onto the stent is still neglected. Moving from such considerations, in this study, we simulate by means of FEA the apposition of a SAPIEN valve in a patient-specific aortic root model accounting for several steps characterising the procedure, i.e. (i) from crimping to deployment and (ii) the leaflet within the metallic frame. Using such a novel simulation strategy, we investigate crucial aspects of TAVI and the impact of prosthesis positioning on its post-implant competence.

2. Materials and methods

The simulation procedure is considerably complex and can be summarised in seven principal steps:

(1) creation of stent model,
(2) simulation of stent crimping,
(3) creation of the aortic root model,
(4) simulation of balloon inflation and stent expansion,
(5) creation of prosthetic valve model,
(6) simulation of valve mapping onto the deployed stent and
(7) simulation of valve closure.

Each step is detailed below.

2.1 Step 1: creation of stent model

In the absence of both a device sample and design data from the manufacturer, we based the creation of the stent geometry on the few data and pictures available on the official website of the Edwards Lifesciences.

In this study, due to the dimensions of the considered patient's aortic root, we chose a computed tomography-angiography (CT-A) DICOM images, we chose a prosthesis size, which is not present in the market, slightly larger than the two devices (size 23 and 26) proposed on the Edwards website.

Moreover, for the sake of simplicity, assumptions were made about the geometry of the prosthesis. For example, we did not reproduce in our model the stent holes designed for sewing purposes. Moreover, rounds and bevels were estimated.

We first created the net of the stent using Rhinoceros software v.4.0 (McNeel & Associates, Seattle, WA, USA), observing that a primitive geometry, represented in Figure 1(a), was mirrored and replicated. In Figure 1(b), the net of the stent is represented, and the main dimensions are reported.

Once the unfolded geometry of the stent was created, we meshed it using Abaqus software v. 6.10 (Simulia, Dassault Systéms, Providence, RI, USA), obtaining a list of nodes and elements. To such nodes, we assigned proper polar coordinates easily computed from their original Cartesian coordinates to obtain the folded geometry depicted in Figure 1(c).

The stent was discretised using 90,279 solid elements with reduced integration (C3D8R). The material used for the balloon-expandable stent is the low carbon 316L stainless steel, whose behaviour is described by an elastoplastic model according to the work of Auricchio et al. (2001).

2.2 Step 2: simulation of stent crimping

A cylindrical catheter was gradually crimped leading to stent deformation. The initial diameter of the catheter was 28 mm whereas the final diameter was 7 mm, in agreement with the work of Capelli et al. (2010): the stent undergoes large deformations as highlighted in Figure 2 where the first and last crimping phases are shown.

A quasi-static simulation was carried out using Abaqus/Explicit; the kinetic energy was monitored to ensure that inertial effects do not affect the results. The catheter was meshed using 403 4-node surface elements with reduced integration (SFM3-D4R), and it was modelled as a rigid material. A frictionless general contact was used to handle the interactions between the catheter and the stent.

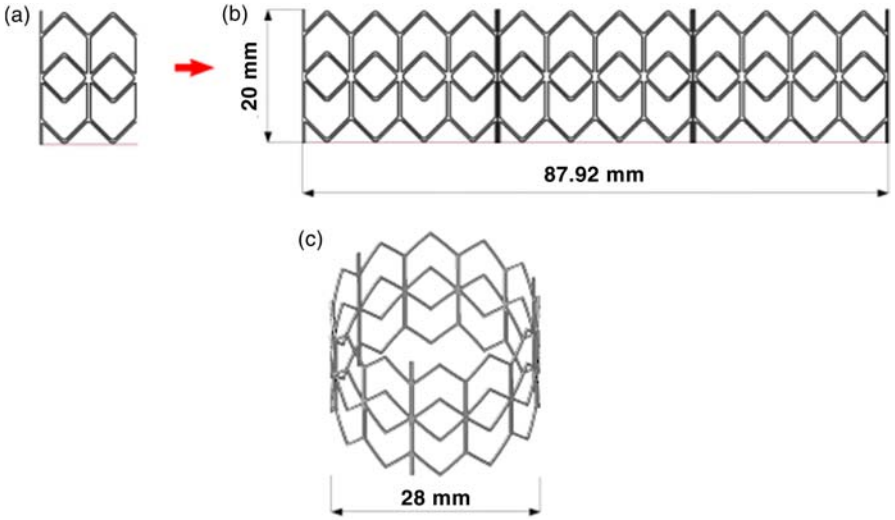

Figure 1. Creation of stent model: (a) a primitive geometry is mirrored and replicated to obtain the model; (b) whole planar model: the stent circumference and height are reported; (c) the nodes of the planar configuration are then expressed in terms of polar coordinates to get the characteristic circular shape: the inner diameter is indicated.

2.3 Step 3: creation of the aortic root model

The aortic root model was obtained by processing the DICOM images of a cardiac computed tomography-angiography (CT-A) carried out using an iodine-contrast dye on a 46-year-old male patient, who provided a written informed consent prior to undergoing a CT scan. The CT-A scan was carried out at IRCCS Policlinico San Matteo, Pavia, Italy, using a SOMATOM Sensation Dual Energy scanner (Siemens Medical Solutions, Forchheim, Germany). The scan data were characterised by the following features: slice thickness, 0.6 mm; slice width × height, 512 × 512 and pixel spacing, 0.56 mm.

The processing procedure was carried out moving from end-diastolic data; OsiriX software v. 3.9 (Rosset et al. 2004) was used to extract a stereolithographic representation (STL) of the aortic root under investigation (see Figure 3(a)). The obtained STL file was elaborated using Matlab (The Mathworks Inc., Natick, MA, USA) to generate the aortic root mesh: we first defined a set of closed lines representing the cross-sectional profile of the inner aortic root wall, the outer profile was then reconstructed imposing a radial shift of the inner profile considering a uniform thickness of 1.3 mm (Beck et al. 2001) (see Figure 3(b)). The final step consisted in defining the hexahedral-element mesh (C3D8R Abaqus elements) between the inner and outer boundaries as depicted in Figure 3(c).

The aortic root wall was modelled adopting realistic constitutive laws, accounting for non-linearity and anisotropy: the aortic sinuses are, in fact, made of a fibre-reinforced material in which the fibres, corresponding

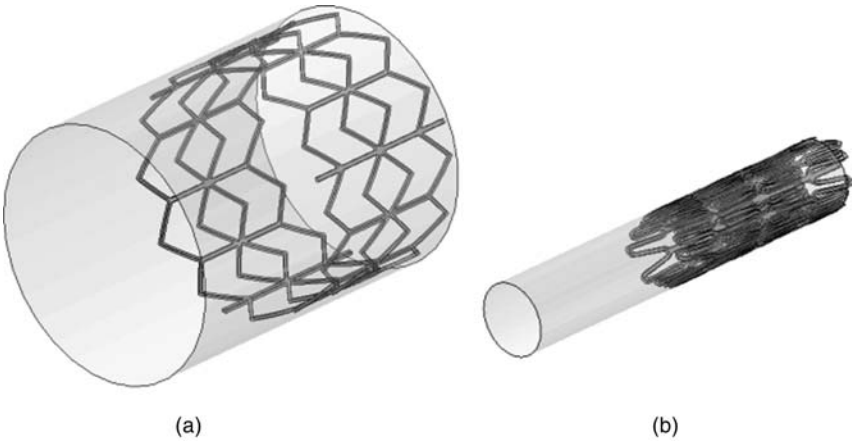

Figure 2. Simulation of stent crimping: (a) at the beginning a rigid catheter is created around the undeformed geometry of the stent; (b) the catheter is gradually crimped leading to stent deformation.

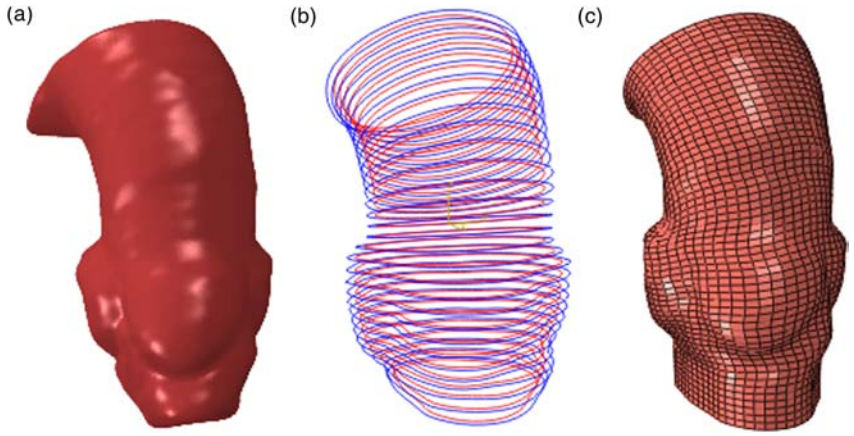

Figure 3. Creation of aortic root model: (a) an STL file is extracted by processing the DICOM images; (b) the inner (red) and outer (blue) lines identifying the aortic root wall are defined from the STL file; (c) a hexahedral element mesh is then created.

to the collagenous component, are embedded in an isotropic hyperelastic matrix of elastin.

Several constitutive laws of arterial tissue are available in the literature based on large deformation theory and accounting for fibres. In this study, we adopted the model proposed by Holzapfel et al. (2000) because it is available in the material library of Simulia (2010).

The adopted strain energy function reads:

$$\Psi = c_{10}(I_1 - 3) + \frac{k_{1i}}{2k_{2i}} \sum_i \left\{ \exp[k_{2i}(\kappa I_1 + (1-3\kappa)I_{4i} - 1)^2] - 1 \right\}, \quad i = 1,2, \tag{1}$$

where I_1 is the first invariant of the right Cauchy–Green deformation tensor $\mathbf{C}$, c_{10} is related to the mechanical response of the non-collagenous matrix, κ represents the dispersion of the fibres, whereas parameters $k_{1i} > 0$ and $k_{2i} > 0$ are associated with the response of the ith collagen fibre.

It is worth noting that the invariant I_{4i} measures the square of the stretch along the ith preferred direction identified by the unit vector a_{0i}. In particular, it is defined as follows:

$$I_{4i} = \mathbf{C} : \mathbf{a}_{0i} \otimes \mathbf{a}_{0i}. \tag{2}$$

The dispersion of the fibres is assumed to be negligible, i.e. $\kappa = 0$, which means that the fibres are perfectly aligned. Because the two fibre families are mechanically equivalent, we have $k_{11} = k_{12} = k_1$ and $k_{21} = k_{22} = k_2$.

As no information on the collagen fibre orientation is available for the investigated material, we also assumed the angle β, defining such an orientation to be an unknown parameter. It follows that the model of Equation (1) is characterised by four independent parameters, i.e. c_{10}, k_1, k_2 and β, which are calibrated on the experimental data obtained from biaxial tests, recently reported by Martin et al. (2011).

The calibration was carried out using the standard optimisation technique which required the minimisation of the objective function χ^2 defined as the squared sum of the differences between the experimental data and the related model prediction variable:

$$\chi^2 = \sum_{a=1}^{p} \left[\left(\sigma_{11_a}^{\text{mod}} - \sigma_{11_a}^{\text{exp}} \right)^2 + \left(\sigma_{22_a}^{\text{mod}} - \sigma_{22_a}^{\text{exp}} \right)^2 \right] \tag{3}$$

with p being the number of data points.

Superscripts ‘mod’ and ‘exp’ stand for model prediction and experimental measurements, respectively. The results of the fitting procedure are illustrated in Figure 4, whereas the obtained model coefficients are $c_{10} = 29.5\,\text{kPa}$, $k_1 = 148.5\,\text{kPa}$, $k_2 = 484.28$ and $\beta = 40°$.

2.4 Step 4: simulation of balloon inflation and stent expansion

The simulation of stent apposition was carried out by assembling the following: (i) the crimped stent, whose tensional state was imported from the crimping simulation and was assumed as a predefined field, (ii) the balloon was modelled as a cylindrical folded body with two conical tapered ends and (iii) the patient-specific aortic root. The whole assembly is shown in Figure 5.

The balloon model was discretised using 13,680 3-node membrane elements (M3D3); the Duralyn material properties were assigned (De Beule 2008) and a uniform thickness of 0.04 mm was considered.

Once the balloon-stent system was properly placed inside the aortic root model, the Abaqus/Explicit solver was again used to carry out the expansion simulation: a uniform pressure of 1 MPa was gradually applied to the inner surface of the balloon, whereas its fixation to the

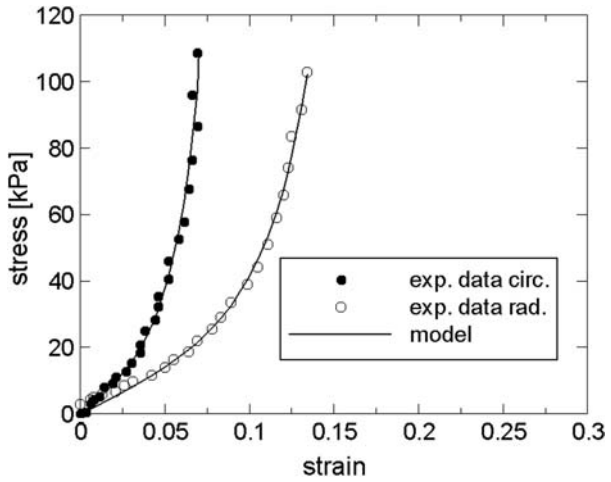

Figure 4. Experimental data versus model prediction: circumferential and radial stress–strain responses of human aortic sinuses (Martin et al. 2011) are compared with results obtained with the model by Holzapfel et al. (2000).

catheter was virtually reproduced by constraining the displacements in each direction of the proximal and distal balloon tips. The complex contact problem of the balloon interacting with itself and the stent is described by a Coulomb friction model with a friction coefficient of 0.2.

2.5 Step 5: creation of prosthetic valve model

The prosthetic valve model was generated through a lofting procedure starting from the circular line of the bottom and the peculiar line of the top of the valve extracted from the real device picture available on the official website of the Edwards Lifesciences (see Figure 6(a)). The two closed lines have to be concentric and, in particular, the top line has to be inscribed into the circular base, whose radius is equal to the inner radius of the stent as shown in Figure 6(b). The obtained leaflet surface was meshed using 8619 shell elements S4R. A uniform thickness of 0.5 mm was assigned to the shell elements.

The valve leaflets are made of glutaraldehyde-treated bovine pericardium which we modelled as an isotropic material following the theses proposed by Lee et al. (1989) and Trowbridge et al. (1985).

Specifically, we considered a simple isotropic nearly incompressible hyperelastic material exploiting a linear relationship between the Cauchy stress and the logarithmic strain measures and characterised by a Young modulus of 8 MPa, a Poisson ratio of 0.49 and a density of 1100 kg/m^3: such values are within the statistical range of the fixed pericardial tissue (Zioupos et al. 1994; Xiong et al. 2010).

2.6 Step 6: simulation of valve mapping onto the deployed stent

Once the simulation of balloon expansion was completed and the stent placed within the aortic root, we carried out a quasi-static simulation to map the valve onto the implanted stent. In particular, we computed the displacement field of two different sets of valve nodes: (i) the nodes lying on the line of attachment with the stent and (ii) the nodes on the circular base of the valve.

Such computed displacements represent the boundary conditions to be applied to the appropriate valve nodes in order to carry out the mapping procedure.

Finally, the overlapping nodes of the stent-valve system were tied together. The result of the mapping operation is shown in Figure 7.

2.7 Step 7: simulation of valve closure

The last step of the procedure to simulate TAVI consists in the simulation of valve closure with the aim of evaluating its performance. The diastolic phase of valve closure was reproduced by gradually applying a uniform pressure of

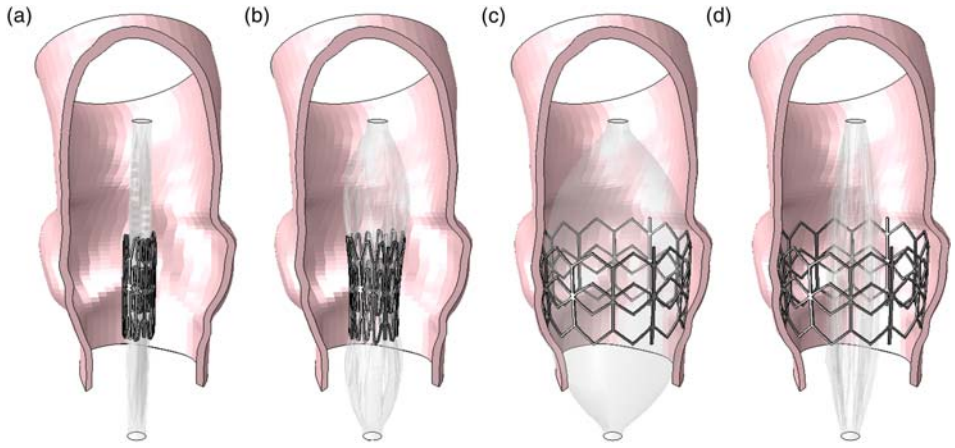

Figure 5. Different frames of balloon expansion and stent apposition: (a) initial configuration; (b) the balloon starts to deploy the stent; (c) the balloon is fully expanded and the stent fully deployed; (d) final configuration after balloon deflation.

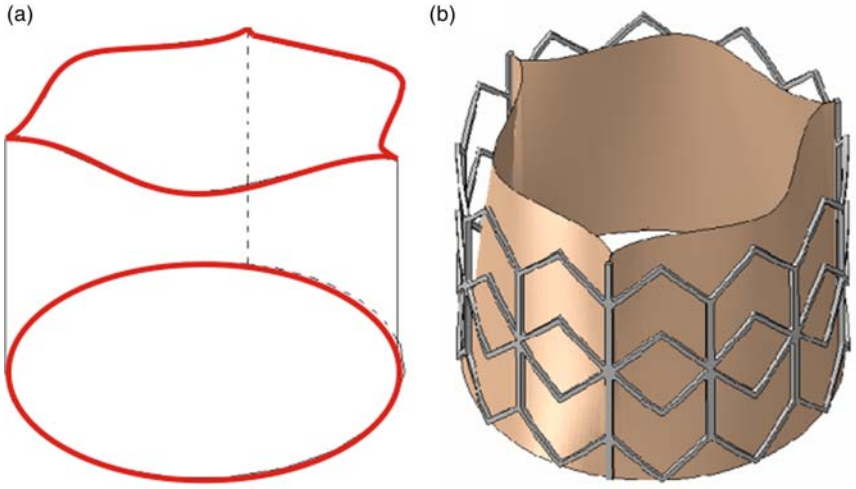

Figure 6. The Edwards SAPIEN model: (a) the valve is created by means of a lofting procedure carried out between the bottom and top curve highlighted in red; (b) the whole device model made of the stent and the valve is shown.

0.01 MPa to the leaflets. The nodes of the aorto-ventricular junction and of the sino-tubular junction belonging to the patient-specific aortic root model were constrained; the displacements of the nodes at the base of the valve were also constrained.

The numerical analysis of the prosthesis closure is a highly nonlinear problem involving large deformations and contact. For this reason, the Abaqus/Explicit solver was used to carry out the simulations; particularly, quasi-static procedures were used, assuming that inertial forces do not affect the solution. Kinetic energy was monitored to ensure that the ratio of kinetic to internal energy remains below 10%.

To neglect peak values of the stress state which can be affected by local effects, we considered only the 99th percentile with respect to the original leaflet area (i.e. we neglected the 1% of the area characterised by the highest stress values), and we computed the average stress, σ_{av}, as follows:

$$\sigma_{\text{av}} = \frac{\sum_{i=1}^{N} \sigma_i A_i}{\sum_{i=1}^{N} A_i}, \tag{4}$$

where σ_i is the stress evaluated at the integration point of each element, A_i is the element area and N is the number of considered elements.

3. Results

The simulation procedure described in Section 2 was carried out in two different cases: particularly, we explored the implications related to the Edwards SAPIEN positioning by focusing on two different implantation sites.

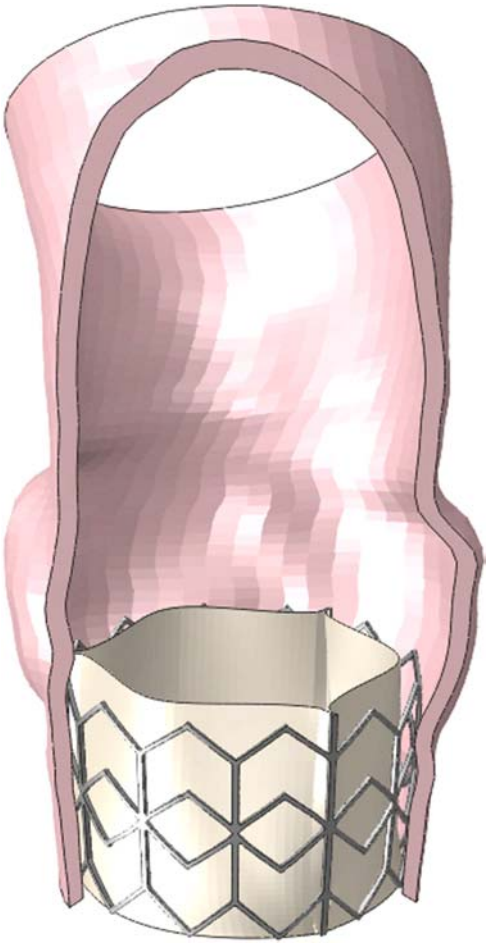

Figure 7. The implanted Edwards SAPIEN device: after carrying out a mapping procedure to map the valve leaflets onto the stent, we obtain the model of the whole transcatheter device implanted in the patient-specific aortic root.

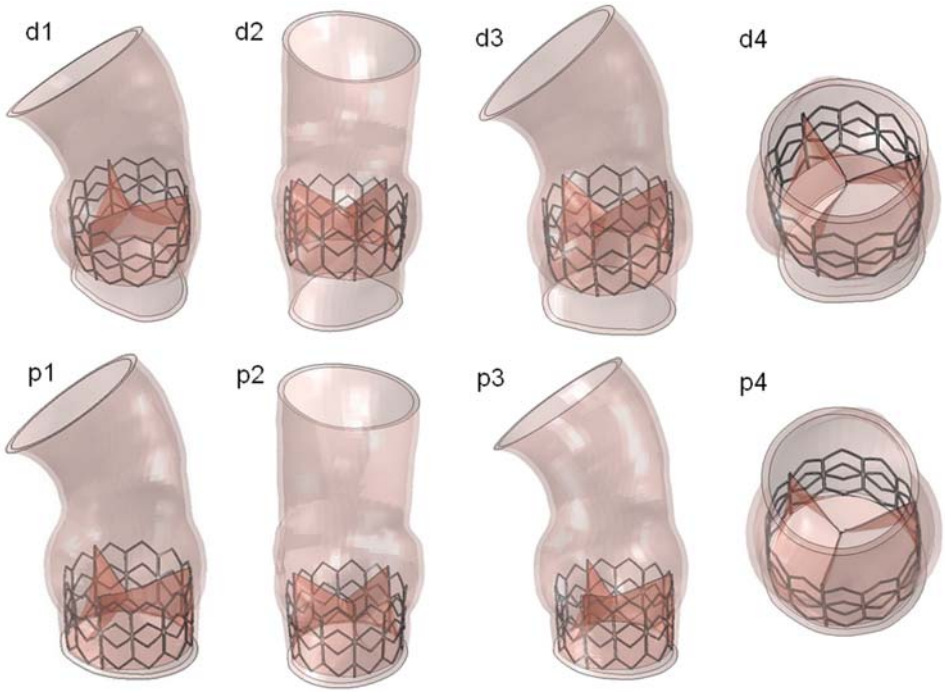

Figure 8. Different views of the implanted transcatheter valve: (d1–d4) the distal positioning; (p1–p4) the proximal positioning.

From the same patient-specific aortic root model, we simulated TAVI both proximally and distally, i.e. in the first case, immediately below the coronary ostia and, in the second case, 7 mm below the distal position. Different views of the two configurations are represented in Figure 8.

The post-operative valve performance was then evaluated in terms of coaptation area (i.e. the total area of the leaflet elements in contact) and stress distribution on the leaflets, as highlighted in Figures 9(a),(b).

The value of σ_{av} in the proximal position is equal to 229 kPa versus an average von Mises stress value in the distal position of 260 kPa, which means that a 13.5% increase of σ_{av} can be observed when moving from a proximal implant approach to a distal approach. The maximum predicted von Mises stress values are equal to 2.32 MPa (proximal configuration) and 2.16 MPa (distal), both below the ultimate stress of bovine pericardium (Sung et al. 1999).

We measured a coaptation area of 340.5 mm^2 for the closed valve placed in the proximal position, whereas the valve positioned distally showed a reduced coaptation area of 258.2 mm^2. In this case, we registered a 24.2% decrease from the proximal implant to the distal implant.

Moreover, the stress induced by balloon inflation both on the stent structure and on the aortic root wall was analysed. As shown in Figure 10(a) and (b), the distal positioning led to reduced stresses on the aortic root wall when compared with the proximal positioning (−22.4%), whereas no significant differences were highlighted looking at the stress state on the stent struts (+0.3%).

The obtained results in the two investigated configurations are summarised in Table 1.

4. Discussion

TAVI is becoming a valuable alternative to classical open-chest surgery for aortic valve replacement, especially for old patients (Leon et al. 2010). Unfortunately, its long-term efficacy and durability are still a matter of debate (Webb et al. 2007), calling for a better understanding of its current drawbacks and of the underlying mechanics. In this scenario, advanced computational techniques may play a crucial role not only as an integral part of the design process, but also to predict post-operative prosthesis performance and, consequently, to help surgeons in identifying the optimal device for a specific patient. For this reason, we integrated CT images and FEA, developing a computational framework which was able to simulate the whole implantation procedure and to predict the interaction between the Edwards SAPIEN transcatheter valve and the patient-specific aortic root anatomy. Moreover, we included in the simulation, the model of the biological valve prosthesis sewn onto the metallic frame; this modelling feature is, to the best of our knowledge, not available in the recent studies investigating the structural behaviour of TAVI through FEA

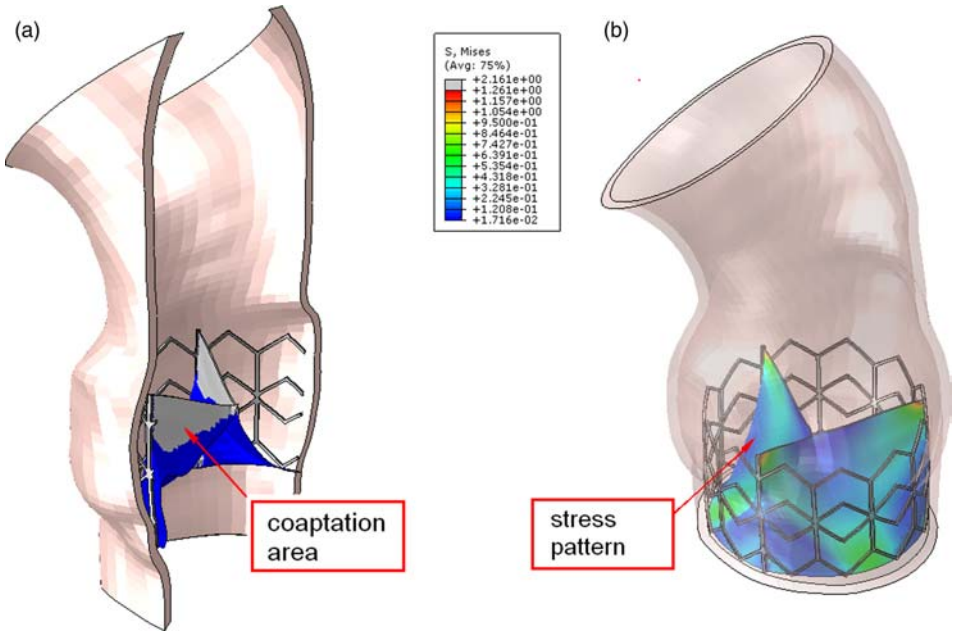

Figure 9. Simulation results: (a) the coaptation area is highlighted; (b) the leaflet tensional state (MPa) is reported.

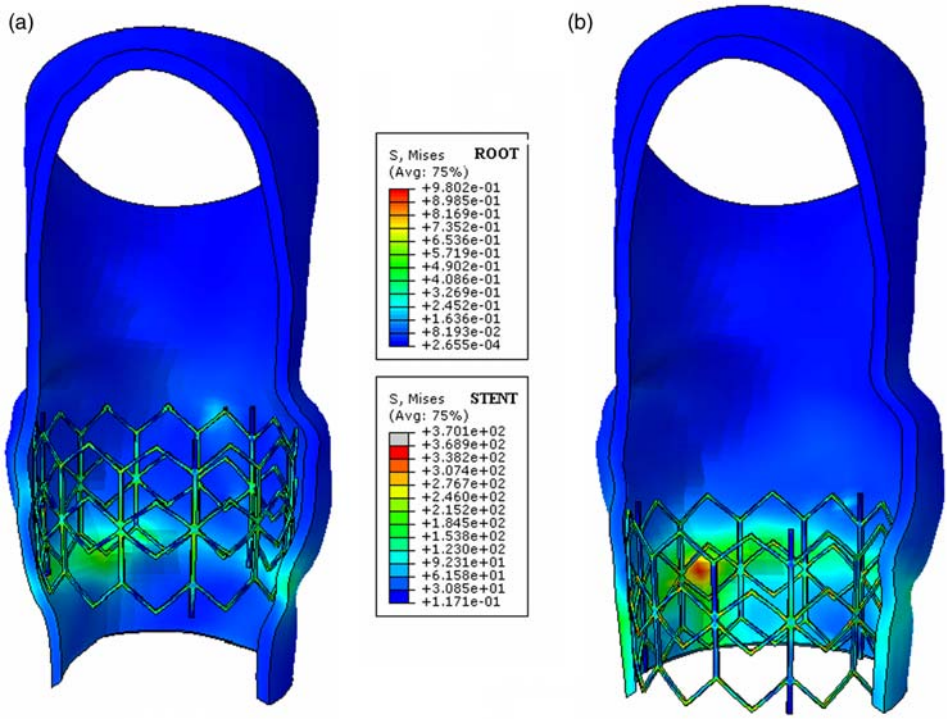

Figure 10. Simulation results: the von Mises stresses on the aortic root wall and stent struts are represented (a) after the distal positioning and (b) after the proximal positioning.

(Capelli et al. 2012; Tzamtzis et al. 2012; Wang et al. 2012). The inclusion of the prosthetic leaflets allows computation of the post-implant valve performance, evaluated in terms of coaptation area and stress/strain field; the former gives a direct anticipative indication of the efficacy of the non-invasive repair procedure, whereas the latter highlights localised stresses/strains on the prosthesis, identifying the weakest point of the implanted

Table 1. Results of prosthesis performance simulation.

	Coaptation area leaflets (mm^2)	Average stress, σ_{av} leaflets (kPa)	Maximum von Mises stress on leaflets (MPa)	Maximum von Mises stress on aortic root wall (MPa)	Maximum principal stress on aortic root wall (MPa)	Maximum von Mises stress on Stent struts (MPa)
Proximal	340.5	229	2.16	0.98	0.94	368.9
Distal	258.2	260	2.32	0.76	0.47	370.1
Δ (%)	−24.2	+13.5	+4.5	−22.4	−50.0	+0.3

device. In this study, we focused in particular on the impact of two different implantation sites.

The obtained values of coaptation area and average stress in the two different configurations demonstrated that there were no significant differences in placing the valved stent either proximally or distally, even though we can speculate that the proximal implant should be preferable because it leads to a greater coaptation area, preventing retrograde blood flow and a lower stress, indicating a minor tensional state which can be correlated to prosthesis failure. The end-diastolic average stress on valve leaflets shows good agreement with corresponding stress values on bovine pericardium leaflets presented in other studies (Auricchio et al. 2010; Auricchio et al. 2011; Smuts et al. 2011).

Virtual simulation of the entire transcatheter device, accounting for the prosthetic valve leaflets, implanted in a patient-specific aortic root model represents an essential step also towards the investigation of post-implant haemodynamics and associated migration forces as proved by several recent studies (Dwyer et al. 2009; Azadani et al. 2010; Smuts et al. 2011).

Clearly, the simulation of TAVI allows to evaluate the impact of the prosthesis on the aortic root and the related stress distribution along the vessel wall as depicted in Figure 10. We can observe that a different positioning procedure leads to a different tensional state on the vessel wall, i.e. different potential injury induced by the stent on the aortic root tissue. The obtained stress values, reported in Table 1, are slightly higher than values reported by Capelli et al. (2012) and comparable with the results reported by Wang et al. (2012); obviously, such a difference could be mainly attributable to the different constitutive model assigned to the aortic root.

The analysis of von Mises stress distribution along the prosthesis metallic frame confirms the results reported by Capelli et al. (2012); the final open configuration of the stent is guaranteed by material yielding occurring in correspondence to strut junctions. Moreover, the ultimate stress value of the low carbon 316L stainless steel was not reached, confirming the low risk of acute structural failure after the deployment, although long-term stent failure due to the pulsatile loading conditions during the cardiac cycle cannot be underestimated.

5. Limitations

Despite the discussed computational framework already resembling the complexity of the real TAVI procedure, several steps have to be done to approach the challenge of predicting the clinical outcomes using computer-based simulations as discussed below.

On the one hand, we should create more accurate models of the aortic root; in particular, we may include the native leaflets which will be crushed and compressed by the valved stent. Moreover, we should include valve

calcifications because most of the patients, in whom TAVI is currently used, often present with aortic lesions with severe leaflet calcification showing variability in the bulkiness of the calcific nodules (Padala et al. 2010). Both Wang et al. (2012) and Capelli et al. (2012) proposed a possible modelling for this issue, but, certainly, the limited data in the literature regarding aortic valve calcification material limit the modelling reliability.

We also know that the generation of the aortic root model directly from the CT-A, recorded under physiological pressure, requires to take into account the related pre-tensional state. Despite different approaches being proposed (Alastrue et al. 2010; Gee et al. 2010; Capelli et al. 2012; Wang et al. 2012), it is not clear how to account for heterogeneity of the vessel wall tissue due to presence of calcification. A successful approach could exploit 4D images, thus linking configuration and loading change during the cardiac cycle (Perego et al. 2011).

On the other hand, we should also create a more accurate model of the SAPIEN device, properly modelling all its structural and geometrical details, moving from micro-CT imaging of a real device.

Finally, a dedicated validation of the numerical outcomes with respect to *in vitro* and *in vivo* data (i.e. simulation vs post-operative or follow-up images) will certainly enhance the reliability of the proposed computer-based tools. However, it is also worth emphasising that this study is mainly methodological; its primary aim is to assess a step-by-step strategy for TAVI simulation, which could represent a solid base for further developments directed towards the practical use of simulation as support in procedural planning.

6. Conclusions

Besides the intrinsic limitation related to the complex system under investigation, we may conclude that the proposed methodology offers a useful tool to evaluate a balloon-expandable valve implant aiming at anticipating surgical operation outcomes. In this study, in fact, we demonstrated that through the proposed simulation strategy, it is possible to evaluate and compare different configurations of the Edwards SAPIEN implantation within aortic root geometries. In particular, the proposed computational framework has been addressed to include the following key aspects: (i) patient-specific geometries derived directly from medical images, (ii) realistic simulation of balloon expansion, (iii) aortic root anisotropy and (iv) post-operative performance evaluation of the whole implanted device which include stent and leaflets. For this reason, in our opinion, the developed simulation strategy can represent a first step towards virtual planning of TAVI procedures aiming at improving the efficacy of the surgical technique and supporting device optimisation.

Acknowledgements

This work is partially funded by the Cariplo Foundation through Project no. 2009.2822 and partially by the European Research Council through Project no. 259229 entitled 'ISOBIO: Isogeometric Methods for Biomechanics'.

The authors thank Dr M. Aiello of IRCCS Policlinico San Matteo, Pavia, Italy, for his support on medical aspects related to this work, Dr A. Valentini of IRCCS Policlinico San Matteo, Pavia, Italy, for support on the imaging aspects of this work and Dr Anna Ferrara, Civil Engineering Dept., University of Pavia, Italy, for providing the calibration data of the anisotropic tissue.

References

AHA committee. 2010. Heart disease and stroke statistics 2010 update: a report from the american heart association. Circulation. 121(7):e46–e215.

Alastrue V, Garia A, Pena E, Rodriguez JF, Martinez MA, Doblare M. 2010. Numerical framework for patient-specific computational modelling of vascular tissue. Int J Numer Methods Biomed Eng. 26(1):35–51.

Auricchio F, Conti M, Demertzis S, Morganti S. 2010. Finite element analysis of aortic root dilation: a new procedure to reproduce pathology based on experimental data. Comp Meth Biomech Biomed Eng. 14(10):875–882.

Auricchio F, Conti M, Morganti S, Totaro P. 2011. A computational tool to support pre-operative planning of stentless aortic valve prosthesis. Med Eng Phys. 33(10):1183–1192.

Auricchio F, Di Loreto M, Sacco E. 2001. Finite element analysis of a stenotic artery revascularization through a stent insertion. Comp Meth Biomech Biomed Eng. 4:249–263.

Azadani A, Jaussaud N, Matthews P, Ge L, Chuter T, Tseng E. 2010. Transcatheter aortic valves inadequately relieve stenosis in small degenerated bioprostheses. Interact Cardiovasc Thorac Surg. 11:70–77.

Beck A, Thubrikar M, Robicsek F. 2001. Stress analysis of the aortic valve with and without the sinuses of valsalva. J Heart Valve Dis. 10:1–11.

Capelli C, Bosi M, Cerri E, Nordmeyer J, Odenwald T, Bonhoeffer P, Migliavacca F, Taylor AM, Schievano S. 2012. Patient-specific simulations of transcatheter aortic valve stent implantation. Med Biol Eng Comput. 50:183–192.

Capelli C, Taylor A, Migliavacca F, Bonhoeffer P, Schievano S. 2010. Patient-specific reconstructed anatomies and computer simulations are fundamental for selecting medical device treatment: application to a new percutaneous pulmonary valve. Philos Transact A Math Phys Eng Sci. 368(1921):3027–3038.

Cribier A, Eltchaninoff H, Bash A, Borenstein N, Tron C, Bauer F, Derumeaux G, Anselme F, Laborde F, Leon M. 2002. Percutaneous transcatheter implantation of an aortic valve prosthesis for calcific aortic stenosis: first human case description. Circulation. 106:3006–3008.

Cribier A, Saoudi N, Berland J, Savin T, Rocha P, Letac B. 1986. Percutaneous transluminal valvuloplasty of acquired aortic stenosis in elderly patients: an alternative to valve replacement? Lancet. 1:63–67.

David T, Ropchan G, Butany J. 1988. Aortic valve replacement with stentless porcine bioprosthesis. J Cardiac Surg. 3:501–505.

De Beule M. 2008. Finite element stent design [Ph.D. thesis]. Ghent: University of Ghent.

Dwyer H, Matthews A, Azadani L, Ge L, Guy TS, Tseng E. 2009. Migration forces of transcatheter aortic valves in patients with noncalcific aortic insufficiency. J Thorac Cardiovasc Surg. 138(5):1227–1233.

Edwards Lifesciences. The Edwards SAPIEN valve. Web-page (last accessed on April 2011).

Fann J, Chronos N, Rowe S, Michiels R, Lyons B, Leon M, Kaplan A. 2008. Evolving strategies for the treatment of valvular heart: preclinical and clinical pathways for percutaneous aortic valve replacement. Catheter Cardiovasc Interv. 71(3):434–440.

Gee M, Förster C, Wall W. 2010. A computational strategy for prestressing patient-specific biomechanical problems under finite deformations. Int J Numer Methods Biomed Eng. 26(1):52–72.

Grube E, Laborde J, Gerckens U, Felderhoff T, Sauren B, Buellesfeld L, Mueller R, Menichelli M, Schmidt T, Zickmann B, et al., 2006. Percutaneous implantation of the corevalve self-expanding valve prosthesis in high-risk patients with aortic valve disease: the siegburg first-in-man study. Circulation. 114:1616–1624.

Holmes D, Nishimura R, Feeder G. 1991. In-hospital mortality after balloon aortic valvuloplasty: frequency and associated factors. J Am Coll Cardiol. 17:189–192.

Holzapfel G, Gasser T, Ogden R. 2000. A new constitutive framework for arterial wall mechanics and a comparative study of material models. J Elasticity. 61:1–48.

Iung B, Baron G, Butchart E, Delahaye F, Gohlke-Barwolf C, Levang O, Tornos P, Vanoverschelde J-L, Vermeer F, Boersma E, et al., 2003. A prospective survey of patients with valvular heart disease in Europe: the euro heart survey on valvular heart disease. Eur Heart J. 24:1231–1243.

Lee J, Haberer SA, Boughner R. 1989. The bovine pericardial xenograft: I. effects of fixation in aldehydes without constraints on the tensile viscoelastic properties of bovine pericardium. J Biomed Mater Res. 23:457–475.

Leon MB, Smith CR, Mack M, Miller DC, Moses JW, Svensson LG, Tuzcu EM, Webb JG, Fontana GP, Makkar RR, et al., 2010. Transcatheter aortic-valve implantation for aortic stenosis in patients who cannot undergo surgery. N Engl J Med. 363:1597–1607.

Lichtenstein S, Cheung A, Ye J, Thompson C, Carere R, Pasupati S, Webb J. 2006. Transapical transcatheter aortic valve implantation in humans: initial clinical experience. Circulation. 114(6):591–596.

Lieberman E, Bashore T, Hermiller J, Wilson J, Pieper K, Keeler G, Pierce C, Kisslo K, Harrison J, Davidson C. 1995. Balloon aortic valvuloplasty in adults: failure of procedure to improve long-term survival. J Am Coll Cardiol. 26:1522–1528.

Martin C, Pham T, Sun W. 2011. Significant differences in the material properties between aged human and porcine aortic tissues. Eur J Cardiothorac Surg. 40:28–34.

Masson J-B, Kovac J, Schuler G, Ye J, Cheung A, Kapadia S, Tuzcu ME, Kodali S, Leon MB, Webb JG. 2009. Transcatheter aortic valve implantationreview of the nature, management, and avoidance of procedural complications. JACC Cardiovasc Interv. 2(9):811–820.

Padala M, Sarin E, Willis P, Babaliaros V, Block P, Guyton R, Thourani V. 2010. An engineering review of transcatheter aortic valve technologies. Cardiovasc Eng Technol. 1(1):77–87.

Perego M, Veneziani A, Vergara C. 2011. A variational approach for estimating the compliance of the cardiovascular tissue: an inverse fluid-structure interaction problem. SIAM J Sc Comp. 33(3):1181–1211.

Peterseim D, Cen Y, Cheruvu S, Landolfo K, Bashore T, Lowe J, Wolfe W, Glower D. 1999. Long-term outcome after biologic versus mechanical aortic valve replacement in 841 patients. J Thorac Cardiovasc Surg. 117(5):890–897.

Piazza N, de Jaegere P, Schultz C, Becker A, Serruys P, Anderson R. 2008. Anatomhy of the aortic valvar complex and its implications of transcatheter implantation of the aortic valve. Catheter Cardiovasc Interv. 1:74–81.

Rosset A, Spadola L, Ratib O. 2004. Osirix: an open-source software for navigating in multidimensional DICOM images. J Digit Imaging. 17(3):205–216.

Schievano S, Taylor A, Capelli C, Lurz P, Nordmeyer J, Migliavacca F, Bonhoeffer P. 2010. Patient specific finite element analysis results in more accurate prediction of stent fractures: application to percutaneous pulmonary valve implantation. J Biomech. 43(4):687–693.

Simulia. 2010. Abaqus manual. Providence, RI: Dassault Systems.

Smuts A, Blaine D, Scheffer C, Weich H, Doubell A, Dellimore K. 2011. Application of finite element analysis to the design of tissue leaflets for a percutaneous aortic valve. J Mech Behav Biomed Mater. 4(1):85–98.

Sun W, Li K, Sirois E. 2010. Simulated elliptical bioprosthetic valve deformation: implications for a symmetric transcatheter valve deployment. J Biomech. 43(16):3085–3090.

Sung H-W, Chen W-Y, Chiu C-T, Chen C-N, Liang H-C. 1999. Crosslinking characteristics and mechanical properties of a bovine pericardium fixed with a naturally occurring crosslinking agent. J Biomed Mater Res. 47:116–126.

Trowbridge EA, Black MM, Daniel CL. 1985. The mechanical response of glutaraldehyde fixed bovine pericardium to uniaxial load. J Mater Sci. 20:114–140.

Tzamtzis S, Viquerat J, Yapc J, Mullenc M, Burriesci G. 2012. Numerical analysis of the radial force produced by the Medtronic-CoreValve and Edwards-SAPIEN after transcatheter aortic valve implantation (TAVI). Med Eng Phys. 35(1):125–130.

Wang Q, Sirois E, Sun W. 2012. Patient-specific modeling of biomechanical interaction in transcatheter aortic valve deployment. J Biomech. 45(11):1965–1971.

Webb J, Chandavimol M, Thompson C, Ricci D, Carere R, Munt B, Buller C, Pasupati S, Lichtenstein S. 2006. Percutaneous aortic valve implantation retrograde from the femoral artery. Circulation. 113:842–850.

Webb J, Pasupati S, Humphries K, Thompson C, Altwegg L, Moss R, Sinhal A, Carere R, Munt B, Ricci D, et al., 2007. Percutaneous transarterial aortic valve replacement in selected high-risk patients with aortic stenosis. Circulation. 116(7):755–763.

Xiong F, Goetz W, Chong C, Chua Y, Pfeifer S, Wintermantel E, Yeo J. 2010. Finite element investigation of stentless pericardial aortic valves: relevance of leaflet geometry. Ann Biomed Eng. 38(5):1908–1918.

Zioupos P, Barbenel JC, Fisher J. 1994. Anisotropic elasticity and strength of glutaraldehyde fixed bovine pericardium for use in pericardial bioprosthetic valves. J Biomed Mater Res. 28(1):49–57.